Journal of Inorganic Biochemistry 193 (2019) 31–41

Contents lists available at ScienceDirect

Journal of Inorganic Biochemistry

journal homepage: www.elsevier.com/locate/jinorgbio

Supramolecular redox-responsive substrate carrier activity of a ferrocenyl Janus device

Shengdong Mu[a,b], Qiangjun Ling[a,b], Xiong Liu[a,b], Jaime Ruiz[c], Didier Astruc[c,*], Haibin Gu[a,b,**]

[a] Key Laboratory of Leather Chemistry and Engineering of Ministry of Education, Sichuan University, Chengdu 610065, China
[b] National Engineering Laboratory for Clean Technology of Leather Manufacture, Sichuan University, Chengdu 610065, China
[c] ISM, UMR CNRS N° 5255, Univ. Bordeaux, 33405 Talence Cedex, France

ARTICLE INFO

Keywords:
Janus dendrimers
Ferrocene
β-Cyclodextrin
Host-guest interactions
Redox response

ABSTRACT

Supramolecular Janus compounds have recently attracted increasing attention owing to their dynamic reversible properties, distinct topological structures, and remarkable physicochemical characteristics, e.g., amphiphilicity, heterofunctionality, and high-density of terminal groups. Herein, a new redox-responsive supramolecular Janus device was designed and synthesized involving β-cyclodextrin and 2-fold ferrocene host-guest interactions. The complex formation was analyzed via one-dimensional ^{1}H NMR and two-dimensional Nuclear Overhauser Enhancement Spectroscopy. $FeCl_3$ and ascorbic acid were used as oxidation and reduction triggers, respectively, to modulate the self-assembly behavior in water through complexation/dissociation of β-cyclodextrin inclusion compounds resulting from redox-conversion of the ferrocenyl guest moieties. The redox-responsiveness of the obtained supramolecular micelles was studied via scanning electron microscopy and dynamic light scattering. Substrate-loading ability of the supramolecular micelles was confirmed with Rhodamine B, and the oxidation of ferrocenyl groups led to the release of the loaded cargos. The present work illustrates a valuable design example of supramolecular Janus systems using the host-guest complexation between β-cyclodextrin and ferrocenyl structures. The present supramolecular micelle may be used as a promising molecular vehicle for application in the field of stimuli-responsive drug delivery.

1. Introduction

Janus molecules or devices are asymmetric molecules or macromolecules containing two distinct hemispheres, i.e. with distinct sizes and functionalities. They have recently attracted the specific attention of scientists in various research fields including macromolecular chemistry [1], molecular materials [2,3] and biomedicine [4]. The reported Janus derivatives were innovatively applied in various fields such as thermal actuators [5], ionic liquids [6], catalysis [7], light capture [8], bioimaging [9], optoelectronics [10,11] and drug delivery [12–16]. Unlike conventional symmetric molecules [17], Janus molecules are normally constructed using two distinct hemispheres with different sizes and functionalities, featuring asymmetric structures [1–4].

Owing to their dynamic nature, various supramolecular interactions including hydrogen bonding [18], host-guest complexes [19–21], or metal complexation [22–24] have been widely investigated in macromolecular chemistry and materials in order to enable stimuli-responsive properties. The redox-sensitive host-guest complexation between β-cyclodextrin (β-CD) and ferrocene (Fc) derivative has been first reported in the mid 1980's [25–27], reviewed [28,29] and applied to smart redox devices such as molecular machines [29] and self-healing materials [29,30]. Recently Schmidt et al. have described a redox- and thermo-responsive gated supramolecular star polymers by using the host–guest complexation of a 6-fold β-CD functionalized core molecule and RAFT-derived Fc end modified by poly(*N*,*N*-dimethylacrylamide) (PDMA) and poly(*N*,*N*-diethylacrylamide) (PDEA) linear polymers [31]. Furthermore, β-CD-modified G5 poly(amidoamine) (PAMAM) and adamantane (Ad)-functionalized G3 PAMAM dendrimers with amine termini were synthesized by Shen and Shi et al. [32] and used to fabricate core–shell tecto dendrimers based on the supramolecular host-guest complexation between β-CD and Ad units. These supramolecular devices were effective vehicles used for gene transfection [32]. Along this line, of exceptional interest are supramolecular Janus macromolecules that possess the key asymmetry property of Janus derivatives and dynamic supramolecular host–guest interactions for the purpose of tailoring

* Corresponding author.
** Correspondence to: H. Gu, Key Laboratory of Leather Chemistry and Engineering of Ministry of Education, Sichuan University, Chengdu 610065, China.
E-mail addresses: didier.astruc@u-bordeaux.fr (D. Astruc), guhaibinkong@126.com (H. Gu).

https://doi.org/10.1016/j.jinorgbio.2018.12.018
Received 15 October 2018; Received in revised form 28 November 2018; Accepted 30 December 2018
Available online 11 January 2019
0162-0134/

their properties via external stimuli, e.g. self-assembly behavior.

Among various host–guest inclusion complexes, a typical β-CD/Fc-based molecular recognition system has been used to fabricate a plethora of supramolecular devices [33–39]. β-CD is a cyclic oligosaccharide composed of seven D-glucose repeating units coupled through α-1,4-glucosidic linkages [40–42], and it resembles a truncated-cone construction with hydrophilic outside surface and hydrophobic internal cavity on the truncated cone [40–42]. Especially, β-CD is capable of complexing the sandwich-like hydrophobic Fc moiety at an equivalent molar ratio [43–45]. The formed inclusion complex is dissociated after the neutral hydrophobic Fc is transferred into cationic hydrophilic ferricinium (Fc^+) using chemical oxidants or electrochemical oxidation and recovered upon reduction of Fc^+ back to its original neutral Fc structure [44]. This unique transition has been utilized to construct various redox-responsive supramolecular systems [46–53]. For example, Zhang and Li et al. synthesized Fc modified camptothecin (Fc-CPT) via a dithioether bond and methoxy polyethylene glycol containing β-CD end (mPEG-β-CD). These authors further fabricated Fc-CPT and mPEG-β-CD-based supramolecular micelles possessing dual redox-responsiveness of reactive oxygen species (ROS) and glutathione (GSH) [54]. These spherical supramolecular micelles in water exhibit hydrophobic inner core and mPEG as a hydrophilic outer shell and show remarkable hyper-fast CPT release under tumor cell redox microenvironment [54]. In human cancer cells, there is a higher amount of ROS (such as H_2O_2) than normal cells, which may oxidize Fc into Fc^+ and thus lead to the release of the loaded drugs [54].

Critically, however, no redox-responsive supramolecular Janus dendrimer system has been fabricated using the oxidation and reduction properties of Fc/β-CD complexes. Herein, as shown in Scheme 1, a Janus metallodendrimer **11** was first synthesized by a typical chemo selective coupling route [4] in which two dendrons containing three triethylene glycol (TEG) branches and two Fc termini, respectively, were connected by an ester bond. Fc-terminated dendrons have already been designed and shown to introduce remarkable switching properties in macromolecular devices and ensembles [55–60]. The supramolecular Janus molecule **β-CD@11** (Fig. 1) was then fabricated by simply mixing the Fc-containing Janus molecule **11** with β-CD host molecules by host–guest complexation between β-CD and Fc. The formation of inclusion complex is verified via one-dimensional ^{1}H NMR and two-dimensional nuclear Overhauser enhancement spectroscopy (NOESY). Chemical redox triggers, namely the use of $FeCl_3$ as oxidant and ascorbic acid as reductant, were utilized to control the self-assembly behavior of the Fc-containing supramolecular Janus assembly **β-CD@11** in water via the association/dissociation transition resulting from the redox-conversion of Fc moieties, and the changes of micelles were carefully detected by scanning electron microscopy (SEM) and dynamic light scattering (DLS). Finally, the **β-CD@11** micelles were used as supramolecular carriers to encapsulate Rhodamine B (RhB), and the loaded RhB were released using a chemical oxidation trigger.

2. Experimental

2.1. Synthesis of 11

9 (1.58 g, 2.60 mmol, 1 equiv) was dissolved in 25 ml of dry CH_2Cl_2, and oxalyl dichloride (3.30 g, 26.0 mmol, 10 equiv) was then injected dropwise into the solution at 0 °C under N_2 atmosphere. After the addition, the obtained mixture was agitated at r. t. for 12 h under N_2 atmosphere, and the solvent was then removed in vacuo to yield crude **10**. The product was directly used in the future step, and no further purification was conducted. **5** (0.95 g, 2.6 mmol, 1 equiv) and triethylamine (2.63 mg, 3.62 mmol, 10 equiv) were added into a Schlenk flask and dissolved in 50 ml of dry CH_2Cl_2. 10 ml of dry CH_2Cl_2 was used to dissolve crude **10**, and the solution was injected into the Schlenk flask. This mixture was agitated at r. t. for 12 h under N_2 atmosphere, and 50 ml of distilled water was added. This two-phase mixture was separated using a separating funnel. The under phase was washed with CH_2Cl_2 (3 × 50 ml), and all the CH_2Cl_2 phase was collected and combined in a flask and washed with brine. The residual water in CH_2Cl_2 phase was trapped using anhydrous Na_2SO_4. Next, the insoluble salts were removed by suction filtration, and the solvent of obtained filtrate was removed in vacuo to yield a crude product. Finally, its purification was conducted by column chromatography in which the mixture of CH_2Cl_2 and methanol (50:1, v/v) was used as the eluent. The obtained compound **11** was a yellow-brown solid. Yield: 1.6 g, 48%. ^{1}H NMR (400 MHz, $CDCl_3$, 25 °C, TMS), δ_{ppm}: 7.52 (s, 2H, 2 × C = CH of triazole), 7.29 (s, 2H, ph), 6.62 (d, J = 2.4 Hz, 2H, ph), 6.56 (t, J = 4.0 Hz, 1H, ph), 5.28 (s, 4H, 2 × OCH_2), 5.22 (s, 2H, $COOCH_2$), 5.11 (s, 4H, 2 × NCH_2), 4.26 (t, J = 3.7 Hz, 4H, 2 × sub. Cp), 4.22–4.16 (m, 20H, 3 × ph-OCH_2, 2 × sub. Cp, 2 × free Cp), 3.86–3.51 (m, 30H, 3 × $CH_2OCH_2CH_2OCH_2CH_2$), 3.36 (d, J = 2.0 Hz, 9H, 3 × OCH_3). ^{13}C NMR (100 MHz, $CDCl_3$, 25 °C, TMS), δ_{ppm}: 164.9 (COO), 158.5, 151.3, 142.6, 137.5, 123.8, 108.1, 106.4, 100.5 (ph), 141.7, 121.2 (C of triazole), 79.6 (Cp), 71.3, 70.9, 69.8, 69.6, 69.5, 68.6, 68.1, 68.0, 67.9 (OCH_2 and Cp), 65.4 (CH_2), 61.1 (CH_2), 58.0 (CH_3), 49.1 (OCH_2). MS (ESI m/z), calcd. for $C_{63}H_{80}Fe_2N_6O_{16}$: 1289.05; found: 1289.44 (M^+), 1311.42 ($M + Na^+$). Selected IR (KBr, cm^{-1}): 3445 cm^{-1} (ν_{OH}), 2924 cm^{-1} (ν_{CH2}), 1430 cm^{-1} (ν_{N3}), 1715 cm^{-1} ($\nu_{C=O}$), 1634 cm^{-1} ($\nu_{C=C}$), 1105 cm^{-1} (ν_{C-O-C}), 823 cm^{-1} (ν_{Fe}^{II}).

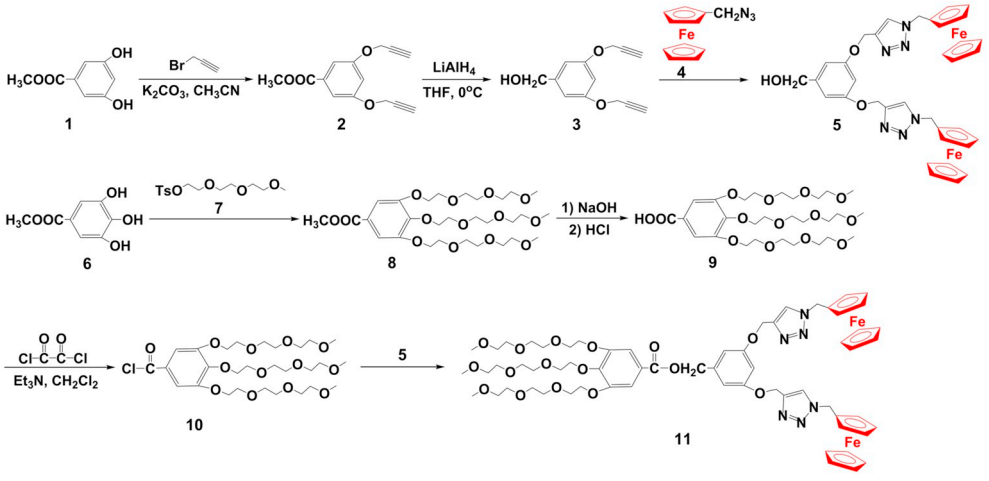

Scheme 1. Synthetic route to the Janus substrate **11**.

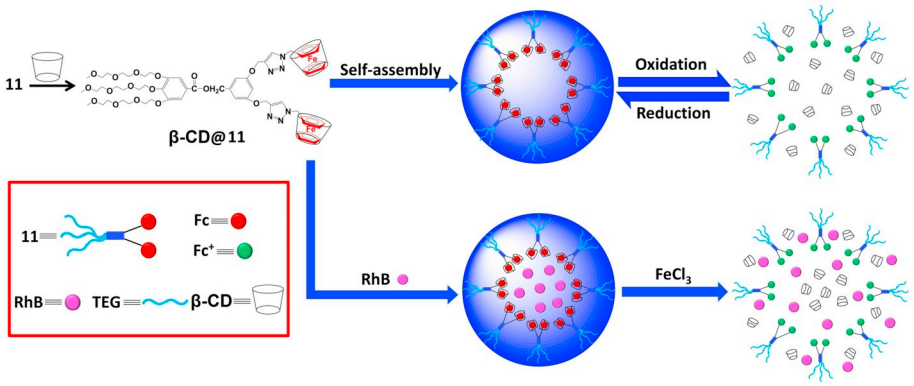

Fig. 1. Schematic formation of the Janus supramolecule **β-CD@11** and its redox-responsive self-assembly, drug-loading and oxidation-triggered release.

2.2. Oxidation of 11 and back reduction

11 (23.3 mg, 0.018 mmol, 1 equiv) was dissolved in 5 ml of methanol, and $FeCl_3$ (11.7 mg, 0.072 mmol, 4 equiv) was then added to oxidize the Fc moieties in **11** to Fc^+ cations. The obtained mixture was stirred for 10 min, and the color of the solution changed from original yellow to pale green. In the following reduction experiment, ascorbic acid (13.95 mg, 0.792 mmol, 4.4 equiv) was used as the reductant and added to the above solution. The final solution was then stirred for another 10 min, and its color changed from pale green to yellow.

2.3. Self-assembly of 11 in water

The dialysis method [68] was utilized to form micellar aggregates of the Janus substrate. 8.0 mg of **11** was thoroughly dissolved in 3 ml of THF, and 1 ml of deionized water was then injected slowly into the solution. Then the mixture was agitated vigorously for 12 h, and the obtained micellar solution was injected into a dialysis bag with molecular weight cutoff (MWCO) of 3500 g mol^{-1} for dialysis treatment [68]. The dialysis bag was then immersed into 1000 ml of deionized water for 72 h in order to completely eliminate the residual THF solvent. During the dialysis process, the dialysate was replaced by fresh deionized water every 5 h [68]. After dialysis, the total volume of aggregate was completed to 4 ml by adding deionized water, and the final concentration of **11** was 2.0 mg ml^{-1}.

2.4. Preparation of the β-CD@11 inclusion complex micelles

β-CD (52.8 mg, 0.0465 mmol, 3 equiv) and **11** (20 mg, 0.0155 mmol, 1 equiv) were initially dissolved using 4 ml and 1 ml of DMF, respectively. The DMF solution of β-CD was then injected dropwise into the DMF solution of **11** under vigorous stirring. The obtained mixture was further heated at 50 °C for 30 h. 2 ml of deionized water was then slowly injected into the DMF solution. Then the obtained micellar solution was injected into a dialysis bag with MWCO of 3500 g mol^{-1} for dialysis treatment. The dialysis bag was then immersed into 1000 ml of deionized water for 72 h in order to completely eliminate the excess β-CD and the residual DMF solvent. After dialysis, the total volume of aggregate was adjusted to 5 ml by adding deionized water, and the final concentration of the inclusion complex was 4.0 mg ml^{-1}.

2.5. Redox-response of micelles of 11 and β-CD@11

The micellar solution of **11** (2 ml, 2.0 mg ml^{-1}, 0.0031 mmol, 1 equiv) was mixed with $FeCl_3$ (2.01 mg, 0.0124 mmol, 4 equiv). The obtained mixture was stirred for 10 min, and the color of the micellar solution changed from the original yellow to pale green. In the following reduction experiment, ascorbic acid (2.40 mg, 0.0136 mmol, 4.4 equiv) was used as the reductant that was added into the above solution. The final solution was then stirred for another 10 min, and its color changed from pale green to yellow. For the micelles of **β-CD@11**, a similar procedure was adopted, and the concentration of the micelles **β-CD@11** was 4.0 mg ml^{-1}.

2.6. Substrate loading of micelles of 11 and β-CD@11

To prepare the RhB-loaded micelles of **11**, 5 ml of micellar solution of **11** (2.0 mg ml^{-1}) and 2.5 mg of RhB were mixed and stirred at r. t. for 12 h. The obtained mixture was then injected into a dialysis bag with MWCO of 3500 g mol^{-1} for dialysis treatment. The dialysis bag was then immersed into 1000 ml of deionized water for 72 h in order to completely eliminate the excess RhB, and the final concentration of **11** was 2.0 mg ml^{-1}. The loading content (LC) and encapsulation efficiency (EE) were estimated using the following formulas [16]:

$$\text{LC}\ (\%) = \frac{W_1}{W_2} \times 100\%$$

$$\text{EE}\ (\%) = \frac{W_1}{W_3} \times 100\%$$

where W_1, W_2, and W_3 are the content of the loaded RhB (mg) by micelles of **11,** the added **11** (mg) and the used RhB (mg), respectively, in the process of encapsulation. The value of W_1 was calculated using the standard curve of RhB (Fig. 9b). A similar procedure was adopted for the RhB-loading of **β-CD@11**, and the final concentration of **11** was 4.0 mg ml^{-1}.

2.7. In vitro oxidation-triggered substrate release from micelles of 11 and β-CD@11

$FeCl_3$ was utilized as the oxidizing agent to initiate the release of RhB from micelles of **11**. Thus 2 ml of the RhB-loaded micelle solution of **11** was injected into a dialysis bag with MWCO of 3500 g mol^{-1} for dialysis treatment. The dialysis bag was then submerged at r. t. into 10 ml of $FeCl_3$ solution with the concentration of 0 and 1.0 mg ml^{-1}, respectively. The titrations by UV − vis. of the oxidant solution were conducted at various intervals outside the dialysis tube, and the release amount of RhB was measured using the standard curve of RhB. A similar procedure was conducted for the in vitro release of RhB from the micelle of **β-CD@11**.

3. Results and discussion

3.1. Synthesis, structure and electrochemical properties of the Janus substrate 11

The targeted amphiphilic Janus molecule **11** is prepared by a typical

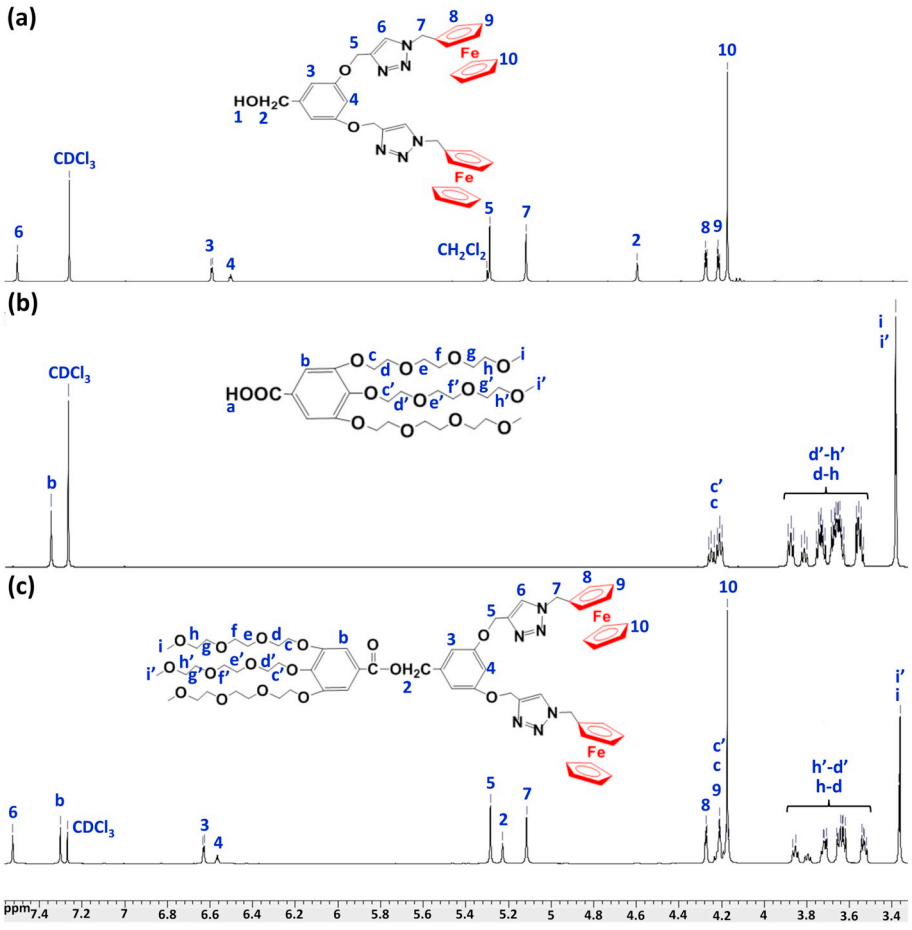

Fig. 2. ^{1}H NMR spectra of **5** (a), **9** (b) and **11**(c) in $CDCl_3$.

chemo selective coupling method [4,69]. As shown in Scheme 1, two dendrons **5** and **9** containing three TEG branches and two Fc termini, respectively, are first synthesized and linked together in the last esterification reaction to yield the new Janus macromolecule **11**. Specially, methyl 3,5-dihydroxybenzoate is used as the starting compound to prepare the hydrophobic dendron **5**. Its reaction with 3-bromo-1-propyne provides the corresponding methyl 3,5-bis(prop-2-yn-1-yloxy) benzoate **2**. $LiAlH_4$ is then utilized to reduce the methyl ester group of **2** to hydroxymethyl group. Next, the obtained compound **3** bearing two terminal alkynyl groups reacts with azidomethylferrocene **4** to yield hydrophobic dendron **5**. This copper(I)-catalyzed azide alkyne cycloaddition (CuAAC) "click" reaction is conducted at r. t. with the aid of the classic Sharpless – Fokin catalyst [70] $CuSO_4$ + NaAsc, and the reaction solvent is the mixture of THF and water (1:1, v/v). The hydrophilic dendron is synthesized by a known procedure [61,62], and its reaction with oxalyl chloride leads to 3,4,5-tris(2-(2-(2-methoxyethoxy) ethoxy)ethoxy)benzoyl chloride **10**. Finally, the novel Janus substrate **11** is fabricated by the reaction between the acyl chloride **10** and the hydrophobic dendron **5** with the aid of trimethylamine. The structure of **11** is verified by ^{1}H (Fig. 2c), ^{13}C NMR (Fig. S14) spectroscopy, mass spectrometry (Fig. S15), UV–vis. (Fig. 3a) and FT-IR spectra (Fig. S16).

Fig. 2 provides the ^{1}H NMR spectra **11** and the two starting dendrons **5** and **9**, and their comparison confirms the structure **11**. As shwon in Fig. 2a, the singlet peak at 7.50 ppm corresponds to the two triazolyl protons, and the appearance of this peak demonstrates the success of the "click" reaction of **3** with **4**. For the two Fc moieties in the structure of **5**, their unique substituted and free cyclopentadienyl (Cp) protons are located at 4.27, 4.21 and 4.17 ppm, and the two peaks at 6.59 and 6.50 ppm are attributed to the phenyl protons. The methyl protons in the CH_2OH group are found at 4.60 ppm, while the two peaks at 5.29 and 5.12 ppm correspond to the CH_2 protons close to the triazole rings (Fig. 2a). These data demonstrate the successful preparation of the Fc-containing dendron **5** and its structure.

As shown in Fig. 2c, no peak is observed at 4.60 ppm for the CH_2 protons close to the OH group, whereas the new peak at 5.22 ppm is assigned to the CH_2 protons connected to the COO group. The above result clearly confirms the successful esterification reaction between the dendrons **5** and **10** yielding **11**. The peak at 7.52 ppm arises from the two triazolyl protons and is not shifted when compared to the corresponding one in Fig. 2a. The multiple peaks at 4.27–4.16 ppm correspond to the substituted and free Cp protons in the two Fc units. They are assigned to the six methene protons adjacent to the phenyl ring. For the three TEG structures, their methylene protons are observed at 3.86–3.51 ppm, and their OCH_3 protons are found at 3.36 ppm. All these results indicate the integrity of the Fc and TEG units and the formation of **11**. Fig. S14 shows the ^{13}C NMR spectrum of **11** in $CDCl_3$. The C=O carbon of the ester group is observed at 164.9 ppm, and its adjacent CH_2 carbon is found at 49.1 ppm. The C=C carbons of the triazolyl units are located at 141.7 and 121.2 ppm, while the Cp carbons of Fc moieties are observed at 79.7, 70.9, 69.6 and 67.9 ppm, respectively. For the TEG units, their terminal OCH_3 carbons are found at 58.0 ppm. As shown in Figs. 2c and S14, all the other peaks are distinctly designated, and they are in accord with the structure **11**. Fig. S15 shows the mass spectrum of **11** in which a molecular peak is observed at 1289.44 Da in accord with the expected value of 1289.05 Da. The UV–vis. spectrum of **11** (Fig. 3a) provides a maximum absorption (λ_{max}) at 435 nm attributed to the d-d* transition of the iron center in the Fc groups. The IR spectrum (Fig. S16) also yields helpful evidence for the formation of **11** with bands at 1715 cm^{-1} ($\delta_{C=O}$), 1596, 1499, 1456 and 1429 cm^{-1} ($\nu_{C=C}$ of benzene), 1375 and 1330 cm^{-1} (ν_{C-N}),

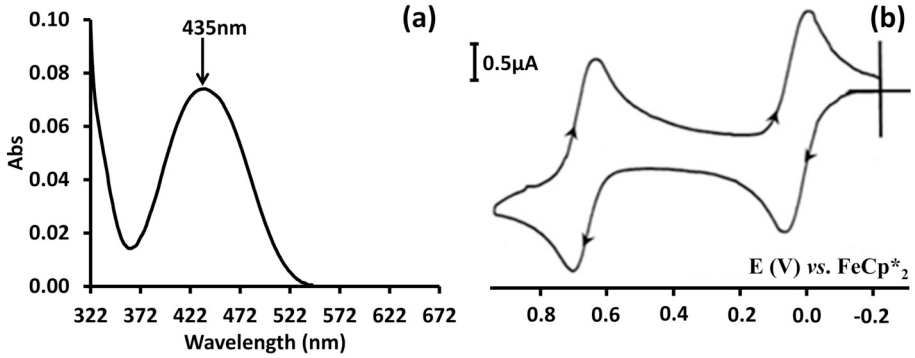

Fig. 3. (a) UV–vis. spectrum and (b) cyclic voltammogram of **11** in CH_2Cl_2 at 20 °C. $FeCp^*_2$ is used as the internal reference (CV wave at 0.0 V). Ag is adopted as reference electrode, and Pt as working and counter electrodes. The scan rate is 0.2 V s^{-1}, and the supporting electrolyte is [*n*-Bu_4N][PF_6] (0.1 M).

1206 and 1106 cm^{-1} (ν_{C-O-C}) and 823 cm^{-1} (ν_{FeII}). The targeted Janus dendrimer **11** is obtained as an orange-yellow thick oil possessing good solubility in usual organic solvents including chloroform, CH_2Cl_2, THF, CH_3CN, acetone, DMF, methanol and dimethyl sulfoxide (DMSO).

Cyclic voltammetry (CV) is adopted to investigate the electrochemical properties of the Fc-containing Janus compound **11** using decamethylferrocene, [$FeCp^*_2$], as the internal reference [63–65]. The CV profile (Fig. 3b) is measured at a scan rate of 0.2 V s^{-1} in CH_2Cl_2 at 20 °C under N_2 atmosphere using [*n*-Bu_4N][PF_6] as the supporting electrolyte [69] and Table 1 provides the $E_{1/2}$ data (measured vs. [$FeCp^*_2$]). For **11**, a single oxidation wave is observed for the Fc redox centers, and the $Fe^{III/II}$ oxidation potential is found at 0.640 V vs. [$FeCp^*_2$] [69]. No adsorption phenomenon is observed in the CV for the ferrocenyl Janus compound **11**. The Fe^{III}/Fe^{II} curve of **11** is chemically ($i_a = i_c$) and electrochemically reversible, although the value of $E_{pa} - E_{pc}$ (0.07 V) is a slightly larger than the known value of 0.059 V for a fast redox process in term of an individual Fc moiety at 25 °C [64,69,71,72]. It could be due to the slight electrostatic factor between the two Fc groups, a known phenomenon [73,74].

The Bard-Anson electrochemical method [66,67,69,75], a method suitable for redox-active Fc-containing polymers and dendrimers with relatively low molecular weight, is utilized to calculate the number of Fc units in **11**. As shown in Table 1, the calculated value of Fc number ($Fc_{experimental}$) for **11** is 2 ± 0.2 (see Table S1 in Supporting Information for details of the measurements), which is in good agreement with the theoretical number ($Fc_{theoretical}$) of 2 calculated by using the targeted structure shown in Scheme 1. In short, the electrochemical determinations fully demonstrate the expected molecular structure of the new Fc-containing Janus molecule **11**.

3.2. Redox reversibility of the bond with the Janus substrate 11

As previously described, the Fc group is transformed into the cationic hydrophilic Fc^+ cation and undergoes reversible redox transformations owing to chemical or electrochemical stimuli [44]. To further prove this point, the Janus compound **11** is chemically oxidized using $FeCl_3$, and the obtained cationic Fc^+-containing Janus molecule is then reduced back to **11** by ascorbic acid following a whole oxidation-reduction circle. The compound **11** in dry methanol is oxidized using two equivalents of $FeCl_3$. In the process of slowly adding the $FeCl_3$ solution, a color change is observed from original yellow to pale green for the solution mixture (Fig. 4), the latter being the typical color of the Fc^+-containing compounds. As expected, the obtained mixture exhibits an absorption band at 630 nm attributed to the unique Fc^+ segment, and in the meantime no peak is observed at 435 nm corresponding to the Fc moiety in the UV–vis. spectrum [16,75,76]. These results further indicate successful oxidation of the Fc group in the Janus compound **11**.

The reduction of the green Fc^+-containing Janus molecule is then carried out stoichiometrically using ascorbic acid as the reductant to yield the original compound **11**. After dropwise addition of the ascorbic acid solution, an obvious color change is found from pale green to yellow (Fig. 4). An absorption peak is observed again at 435 nm, and at the same time the peak at 630 nm disappears. This data proves the reformation of the neutral Fc group. In addition, the slight weakening in absorption intensity at 435 nm is mainly taken into account by the decreased concentration of the recovered compound **11** owing to the addition of solvent employed to dissolve the oxidant and reductant.

Table 1
Redox potentials ($E_{1/2}$), chemical (i_c/i_a) and electrochemical (ΔE) reversibility for **11** and its Fc number determined by the Bard – Anson electrochemical formula.

Dendrimer	$E_{1/2}$[a]	ΔE[b]	i_c/i_a	$Fc_{theoretical}$[c]	$Fc_{experimental}$[d]
11	0.640	0.07	1	2	2 ± 0.2

[a] $E_{1/2} = (E_{pa} + E_{pc})/2$ vs. [$FeCp_2^*$].
[b] $\Delta E = E_{pa} - E_{pc}$.
[c] Expected Fc number of **11** from its targeted molecular structure.
[d] Fc number measured by the Bard – Anson electrochemical formula.

3.3. Self-assembly of 11 in water

The Janus compound **11** contains three hydrophilic TEG branches and two hydrophobic Fc termini, and thus it is anticipated to self-assemble into micellar aggregates in aqueous solution. As shown in Fig. S17, the determined value of critical micelle concentration (CMC) for **11** is 0.447 mg ml^{-1} using the pyrene fluorescence probe technique [68,77]. In the light of this result, the concentration of 2.0 mg ml^{-1} were then employed to explore the self-assembly behavior of **11** in water.

The self-assembly process [76] is studied by slowly adding deionized water into the THF solution of **11**, then the dialysis treatment is conducted to eliminate the residual THF solvent in the solution mixture. The yellow color of the dispersion suggests the formation of micelles, and the self-assembled nanostructures are studied by SEM, atomic force microscopy (AFM) and DLS. The SEM micrograph (Fig. 5a) shows evidence for a nearly spherical morphology of the micelles of **11**, and the determined average diameter is 38 ± 15 nm (Fig. 5b). Besides, the hydrodynamic diameter provided by DLS curve (Fig. 5c) is 176 nm with a polydispersity index (PDI) of 0.096. As expected, DLS technique offers typically larger size of micelles than SEM method owing to their different determination circumstance. In the DLS measurement, the micelles in aqueous solution present the swelling and outstretched state, but SEM yields the size of micellar samples in the dry state [16,68]. Furthermore, the existence of size difference among the SEM and DLS measurements is best taken into account by some aggregation in the aqueous system. This phenomenon is also reflected by the AFM analysis. To prepare the sample for AFM analysis, several drops of micellar

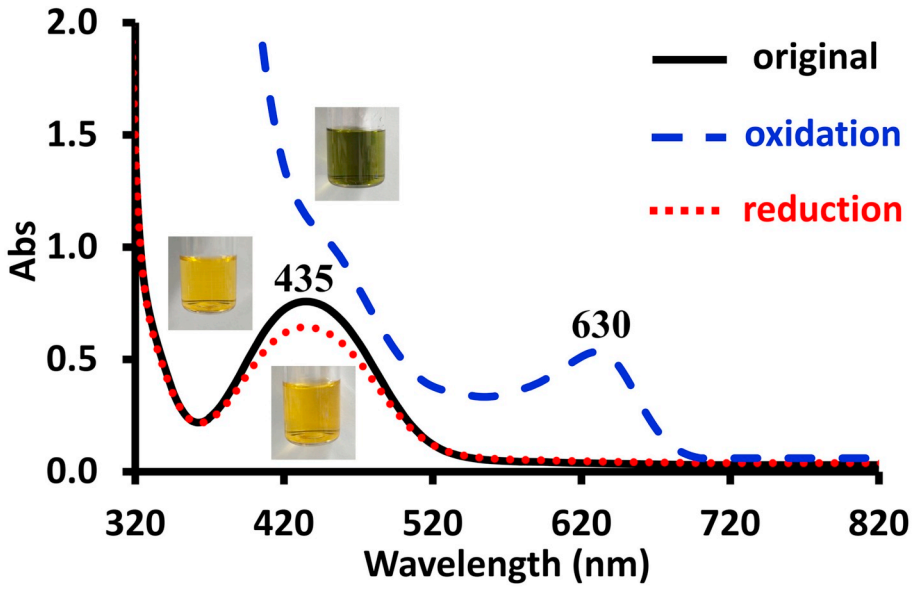

Fig. 4. UV–vis. spectral changes of **11** during an oxidation-reduction cycle.

solution of **11** are casted onto a clean mica substrate. After being dried for 24 h in air, the sample is analyzed using the tapping mode. As shown in Fig. S19, the globular morphology of all the micelles is observed by AFM, and the average particle diameter (D_{av}^{AFM}) of 370 nm is obtained according to the corresponding AFM-based statistical analysis. In short, these results indicate that **11** self assembles into micelles in water.

As described earlier, the Fc units of Janus molecule **11** are reversibly transformed between the oxidation and reduction state. Here, the effect on its self-assembly behavior are further studied using $FeCl_3$ and ascorbic acid as oxidant and reductant, respectively. The redox-responsive experiments are conducted in aqueous system, and the morphologies and sizes of the micelles are monitored by SEM and DLS. Interestingly, for the aggregates **11** near-spherical micelles are still found by SEM (Fig. 5d), but the average size is improved to 104 ± 20 nm (Fig. 5e). The hydrodynamic diameter distributions measured by DLS is about 278 nm with PDI = 0.423 (Fig. 5f). Apparently, the increased average size and the broader scope of size distribution are attributed to the oxidation of the Fc groups to Fc^+ structures. This size increase is likely attributed to the electrostatic repulsion among the positively charged Fc^+ fragments. The reduction

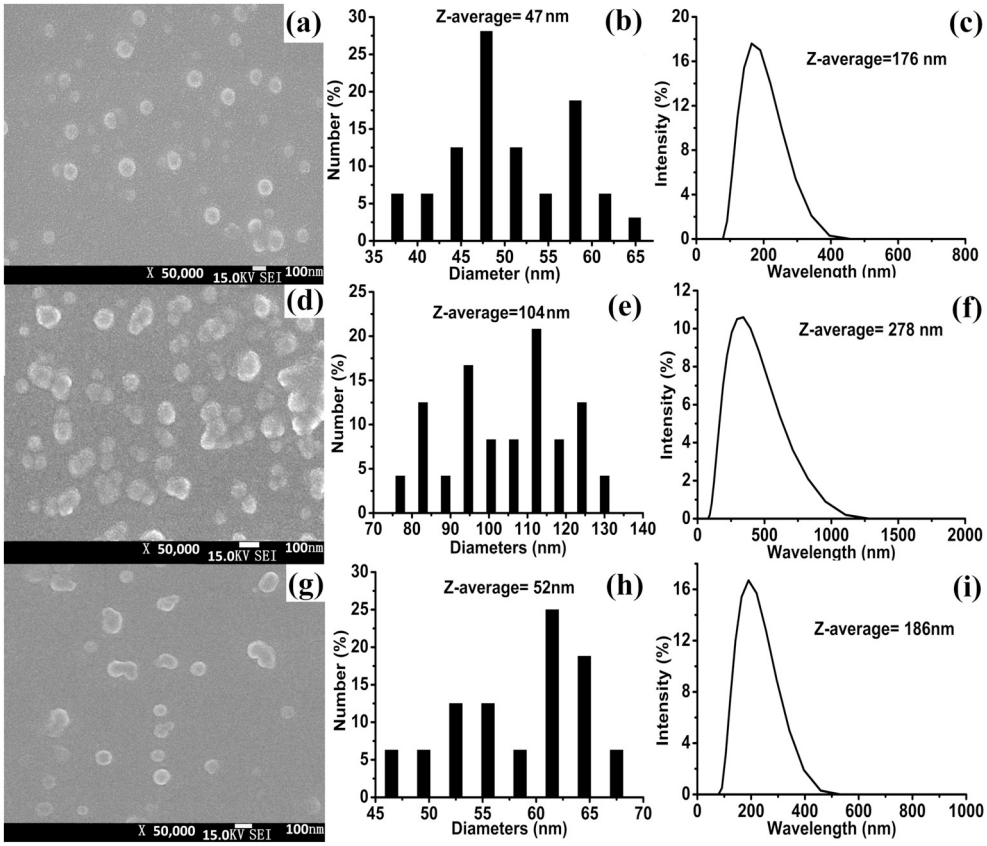

Fig. 5. SEM image (a) and statistical diameter distribution (b) of **11** micelles in water (2.0 mg ml^{-1}), and their size distribution by DLS (c, PDI = 0.096). SEM image (d) and statistical diameter distribution (e) of the oxidized **11** micelles, and their size distribution by DLS (f, PDI = 0.423); SEM image (g) and statistical diameter distribution (h) of the reduced **11** micelles, and their size distribution by DLS (i, PDI = 0.109).

of the oxidized micelles is then conducted by adding ascorbic acid. As anticipated, the micellar size decreases after the addition of ascorbic acid. As shown in Fig. 5g, these re-formed micelles exhibit a spherical shape, and their average size by SEM is 52 ± 15 nm (Fig. 5h), in good agreement with the initial size before oxidation treatment (Fig. 5a). Furthermore, DLS analysis also confirms this reversible change. As shown in Fig. 5i, the recovered micelles exhibit an average hydrodynamic diameter of 186 nm and narrow size distribution indicated by the low PDI of 0.109. These data are consistent with the original value. In a word, according to the results of SEM and DLS, it is clear that the self-assembly process for **11** exhibits reversibility in aqueous solution.

3.4. Substrate loading and oxidation-controlled release from micelles of 11

RhB, a fluorescent molecule, is chosen as model drug to explore the encapsulating ability of micelles formed by Janus molecules **11**. The substrate-encapsulated micelles are prepared by dropwise injecting deionized water into the mixed THF solution of **11** and RhB. After that, the obtained mixture are vigorously agitated at r. t. for 12 h, followed by the dialysis treatment against distilled water to get rid of unencapsulated RhB molecules and remaining THF solvent. The successful encapsulation of RhB by micelles of **11** is demonstrated by the UV–vis. spectrum shown in Fig. S19a. As expected, a new peak attributed to the RhB molecules is observed at 563 nm. The standard profile of RhB (Fig. S19b) is then applied to measure the amount of RhB loaded. The determined values are 0.04% for the loading content and 0.068% for the encapsulation efficiency, respectively.

As shown in Fig. 6a, micelles still exhibit the nearly spherical shape after the encapsulation of RhB. The average diameter evidenced by SEM is 77 ± 30 nm (Fig. 6b), and this value is a little larger than that of pure micelles (Fig. 5b). Moreover, a size of 217 nm is measured by using the DLS profile (Fig. 6c), and the corresponding PDI is 0.245.

The dialysis method was adopted to determine the in vitro release behavior of RhB from micelles of **11**. Concretely, the RhB-loaded micellar solution is dialyzed against the aqueous solution of $FeCl_3$ at 1.0 mg ml^{-1}. At various intervals, a small amount of dialysate is taken out and analyzed using UV–vis. spectroscopy, and the released RhB is calculated using its standard curve [68,76,77]. Fig. 7 shows the release curve of RhB. As expected, the release of RhB from the micelles of **11** is trigged by the addition of $FeCl_3$ at 1.0 mg ml^{-1}. After 20 h of oxidation with $FeCl_3$, the total amount released is 78% or so, and hereafter no further release is observed even after 28 h. During the dialysis treatment by $FeCl_3$, the Fc groups of Janus **11** are converted into cationic Fc^+ structures, and this transformation results in the improvement of coulombic repulsion in the cores of micelles [16]. Thus, the loaded RhB slip out from the enlarged cores of micelles.

3.5. Formation of the supramolecular Janus compound β-CD@11

It is well known that macrocyclic β-CD, as host molecule, has a specific structure with a hydrophilic exterior surface and hydrophobic interior cavity and thus accommodates hydrophobic small molecules such as adamantane, azobenzene and Fc via dynamic non-covalent

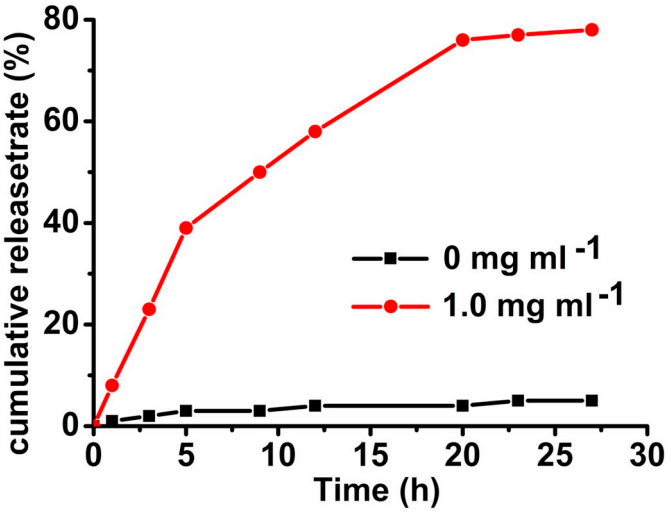

Fig. 7. In vitro release curve of RhB from the micelles of **11** using $FeCl_3$ as oxidant at 0 and 1.0 mg ml^{-1}.

host-guest interactions [40–42,44,76]. Based on this, herein, we further prepare the supramolecular Janus complex **β-CD@11** using the compound **11** and β-CD as the starting materials (Fig. 1). The formation of this supramolecular substrate is confirmed by the results of one- and two-dimensional ^{1}H NMR analysis. Fig. 8 provides the ^{1}H NMR spectra of **11**, β-CD and **β-CD@11**, and their comparison indicates the host-guest interaction between β-CD and Fc units in **11**. As expected, several obvious shift changes are found for the characteristic peaks of β-CD and Fc moieties (Table 2). The peaks at 3.623 and 3.604 ppm are attributed to H-3 and H-5 protons of the β-CD hydrophobic cavity. After mixing β-CD with **11**, the two peaks are found at 3.653 and 3.634 ppm, respectively. Namely, the complexation-induced shift change (Δδ) is 0.030 ppm for both cases. These changes are taken into account by the anisotropic shielding effect [31,78]. For the peaks of the Cp protons in Fc groups, similar shift changes are observed. The corresponding peaks are shifted from 4.328, 4.175 and 4.165 ppm to 4.341, 4.197 and 4.176 ppm, respectively, and the Δδ values are 0.013, 0.022 and 0.011 ppm. These changes indicate that the complexation between β-CD and the Fc units in **11** is successfully achieved.

Nevertheless, for purpose of further confirmation of the well-off construction of **β-CD@11** by supramolecular complexation, 2D-NOESY is chosen for the research of the complex formation. Protons with close proximity in two dimensions exhibit enhanced Nuclear Overhauser Effect (NOE) [31], which typically occurs at distances of 4 Å and lower [31,75,76]. As for the inclusion complexes, the peaks of the host and guest protons are usually found extremely close to present correlation through the NOE [31,78,79]. As shown in Fig. 9, the cross-peaking, protruded by using black squares, are found at the intersection of 3.32–3.67 and 4.10–4.35 ppm, which is attributed to the close adjoining of the Fc moieties and the H3 and H5 protons in the cavities of β-CD, respectively. The appearance of these cross-peaking confirms the

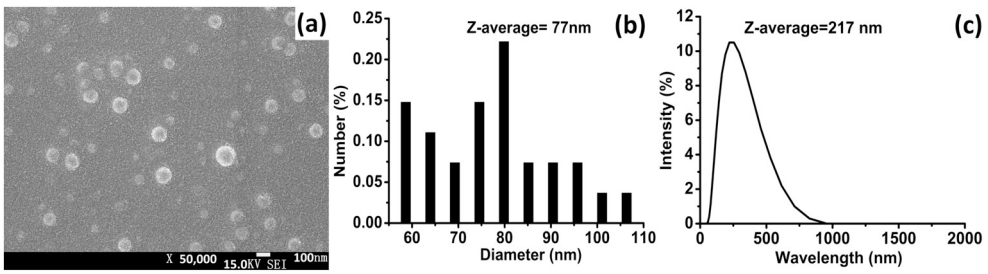

Fig. 6. RhB-loaded **11** micelles: (a) SEM image, (b) histogram of size distribution and (c) DLS curve (PDI = 0.245).

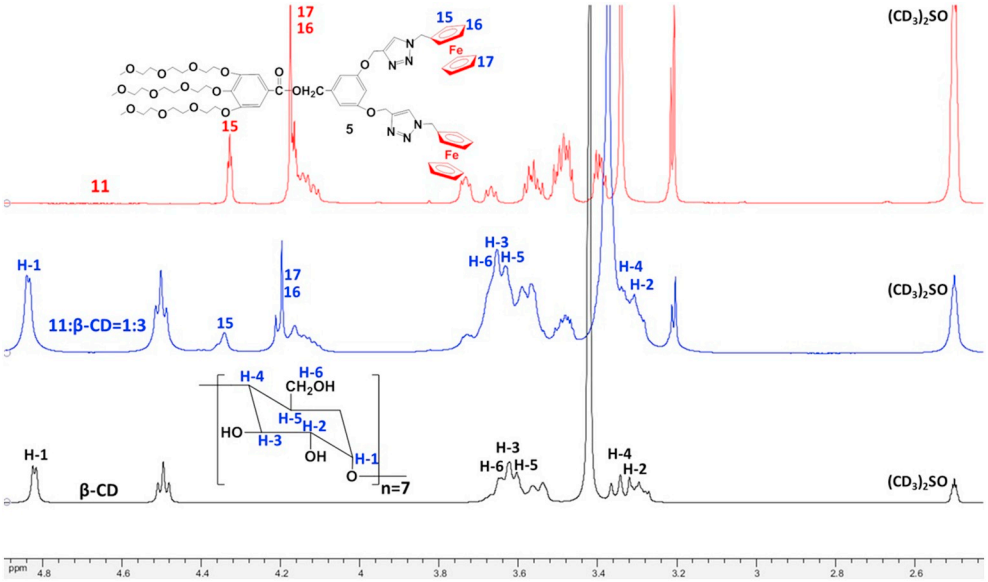

Fig. 8. ^{1}H NMR spectra in DMSO-d_6 of **11**, β-CD and **β-CD@11**.

Table 2
Chemical shifts of β-CD and Fc groups before and after complexation (ppm).

Proton	H-3	H-5	15	16	17
11	–	–	4.328	4.175	4.165
β-CD	3.623	3.604	–	–	–
β-CD@11	3.653	3.634	4.341	4.197	4.176
△δ	0.030	0.030	0.013	0.022	0.011

successful formation of the inclusion complex **β-CD@11**.

3.6. Redox-reversible self-assembly of β-CD@11 in aqueous solution

The pyrene fluorescence probe technique [68,77] is also employed to determine the CMC value of the supramolecular Janus ensemble **β-CD@11**, and the calculated value is 0.661 mg ml^{-1} (Fig. S21). The resulting CMC of **β-CD@11** is higher than that of Janus **11** as a result of its better hydrophilcity than the original Janus molecule **11** [68,77]. On this basis, the concentration of 4.0 mg ml^{-1}, above the CMC of **β-CD@11**, is chosen to investigate its self-assembly behavior.

Like the case of micelles of **11**, the micelles of **β-CD@11** are fabricated using the dialysis method. Concretely, the **β-CD@11** micelles are prepared by slowly injecting deionized water into the DMSO solution of **β-CD@11**. After that, the obtained mixture is vigorously agitated at 30 °C for 24 h, then the excess DMSO solvent is eliminated by the 72 h dialysis against distilled water. The morphology and size of the obtained micelles are well characterized by SEM and DLS. The spherical morphology of **β-CD@11** micelles is confirmed by the SEM image (Fig. 10a), and the corresponding statistic analysis provides an average diameter of 75 ± 20 nm or so (Fig. 10b). As expected, this value is obviously smaller than the size of 450 nm obtained by DLS curve (Fig. 10c), which is attributed to their different testing conditions. The size of **β-CD@11** micelles is moderately larger than that of the corresponding pure micelles of **11**, which is taken into account by the bulky

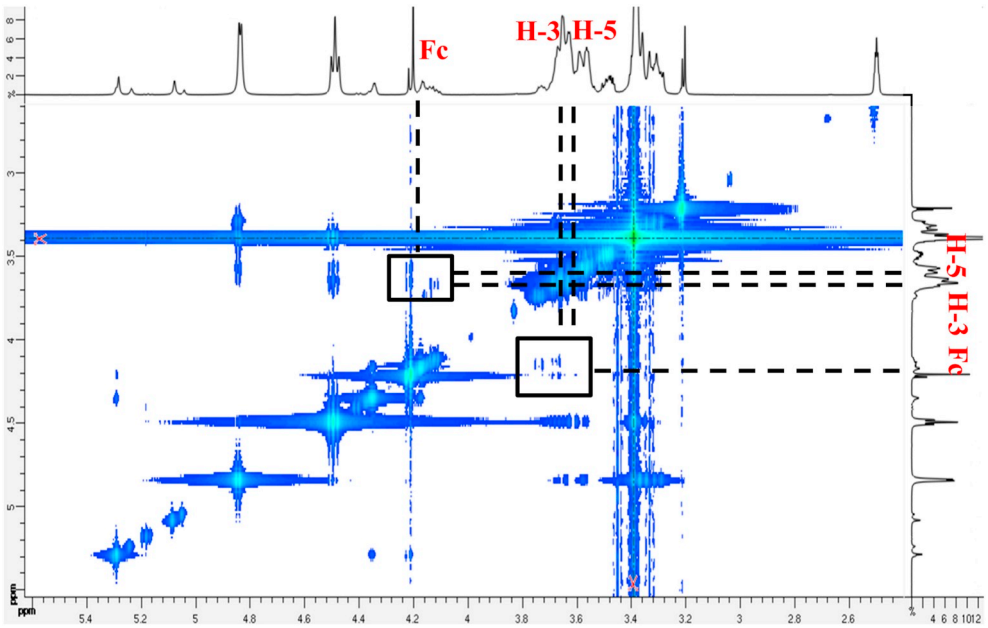

Fig. 9. 2D NOESY NMR spectrum of **β-CD@11** in DMSO-d_6.

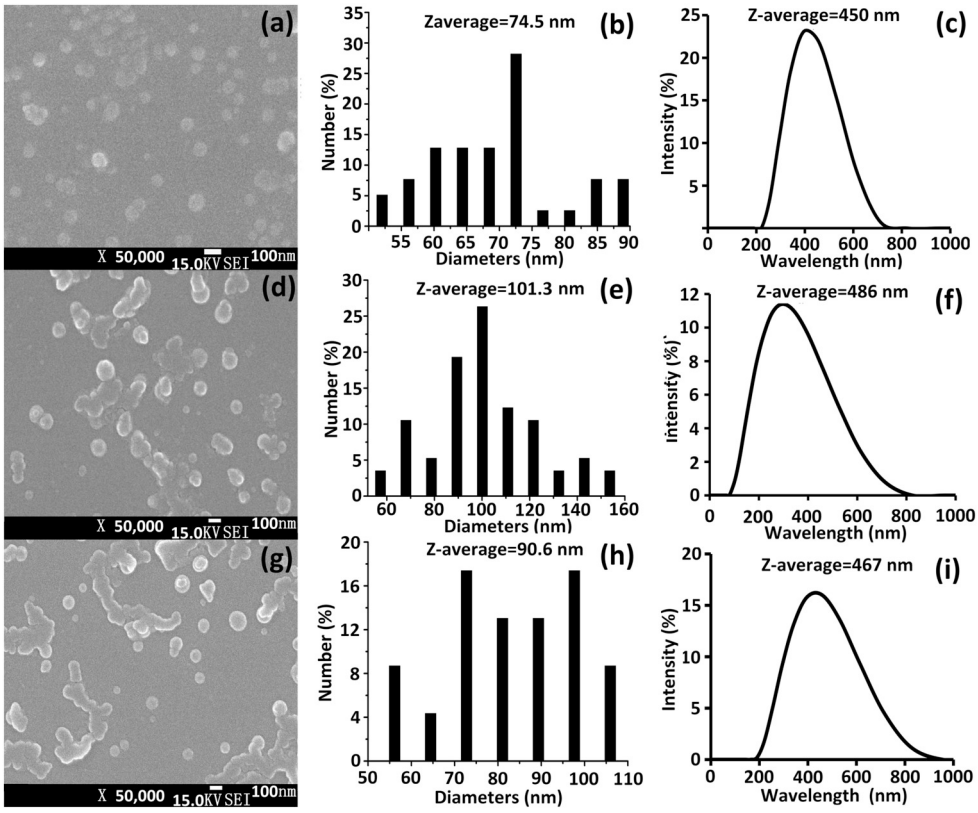

Fig. 10. SEM image (a) and statistical diameter distribution (b) of **β-CD@11** micelles and their size distribution by DLS (c). SEM image (d) and statistical diameter distribution (e) of the oxidized **β-CD@11** micelles and their size distribution by DLS (f); SEM image (g) and statistical diameter distribution (h) of the reduced **β-CD@11** micelles and their size distribution by DLS (i).

inclusion complex of β-CD with Fc units.

Because of the presence of Fc groups, the amphiphilic supramolecular Janus ensemble **β-CD@11** should be redox switchable. Thus, it is interesting to probe the redox-responsive self-assembly behavior of **β-CD@11** through chemical methods. Herein, $FeCl_3$ and ascorbic acid are used as oxidizing and reducing agents, respectively, to carry out the redox reactions [80], and the change of micelles during this process is detected using SEM and DLS techniques. The aggregates **β-CD@11** in the oxidation state still keep the near-spherical morphology, which is evidenced by the SEM image in Fig. 10d. The corresponding statistical analysis yields an average diameter of 101 ± 40 nm or so (Fig. 10e). The hydrodynamic diameter distributions determined by DLS is about 486 nm with PDI = 0.640 (Fig. 10f). Compared to the micelles in original state, these oxidized micelles exhibit an increased size. Apparently, this increase is attributed to the oxidation of Fc into Fc^+. Conceivably, along the oxidation process, the dissociation of the inclusion complexes (β-CD: Fc = 1:1) occurs, and the strong electrostatic repulsion among the Fc^+ fragments further leads to swelling of the micelles (Fig. 1).

The micelle solutions are then reduced by injecting ascorbic acid to test the reversibility of this change. As anticipated, the addition of ascorbic acid results in size decrease of the obtained micelles. As shown in Fig. 10g, the spherical silhouette is still observed for these re-formed micelles, and the average size is reduced to 90 ± 30 nm (Fig. 10h). There is a slight size distinction between the reduced micelles and the original ones before oxidation treatment (Fig. 10a) that is attributable to the presence of residual oxidized micelles. Perhaps, prolonged equilibration treatment leads to inclusion complex re-formation. Therefore, it may be that this process is not perfectly reversible. Furthermore, DLS analysis also indicates the recovery. As shown in Fig. 10i, these recovered micelles exhibit an average hydrodynamic diameter of 467 nm (PDI = 0.603), and this value is almost equal to the original value before oxidation. In short, both SEM and DLS measurements confirm the reversible self-assembly behavior of the supramolecular Janus ensemble **β-CD@11** in water, and this change is successfully fulfilled by redox reactions.

3.7. Substrate-loading and oxidation-triggered release from micelles of β-CD@11

As a model fluorescent molecule, RhB is further employed to study the substrate-loading property of the micelles formed by the supramolecular Janus ensemble **β-CD@11**. The RhB-loaded micelles of **β-CD@11** are prepared by injecting slowly deionized water into the DMSO solution of **β-CD@11** and RhB, then the obtained mixture is vigorously agitated at r. t. for 12 h. The dialysis treatment is then carried out against deionized water to get rid of the remaining DMSO solvent and excess RhB molecules. The successful formation of RhB-loaded micelles of **β-CD@11** is confirmed by UV–vis. spectroscopy. As shown in Fig. S23, the appearance of the characteristic absorption peak at 560 nm indicates the existence of RhB in the obtained micelles. The amount of loaded-RhB is then determined using the standard profile of RhB (Fig. S18b). The obtained values are 1.38% for the loading content and 1.8% for the encapsulation efficiency, respectively. These values are much larger than those obtained for micelles of **11**, indicating the better cargo-loading property of the supramolecular micelles of **β-CD@11**.

The SEM micrograph (Fig. 11a) shows the nearly spherical shape of RhB-encapsulated micelles of **β-CD@11**, and the corresponding statistical analysis provides the average diameter of 110 ± 20 nm (Fig. 11b), which is a little larger than that of empty pure micelles (Fig. 10a). As shown in Fig. 11c, the average hydrodynamic diameter of 500 nm is observed through the DLS analysis, and the corresponding PDI is only 0.143, indicating that these micelles in aqueous system have very narrow size distribution.

The dialysis method is adopted to determine the in vitro release behavior of RhB-containing micelles of **β-CD@11**. Concretely, the RhB-loaded micelle **β-CD@11** is dialyzed against the aqueous solution of $FeCl_3$ at 1.0 mg ml^{-1}. At various intervals, a small amount of dialysate is taken out and analyzed using UV–vis. spectroscopy, and the amount of released RhB is determined using its standard curve [68,76,77]. As

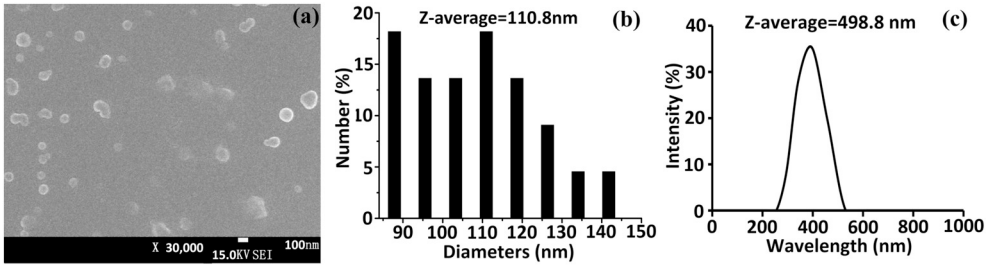

Fig. 11. RhB-loaded micelles **β-CD@11**: (a) SEM image, (b) histogram of size distribution and (c) DLS curve.

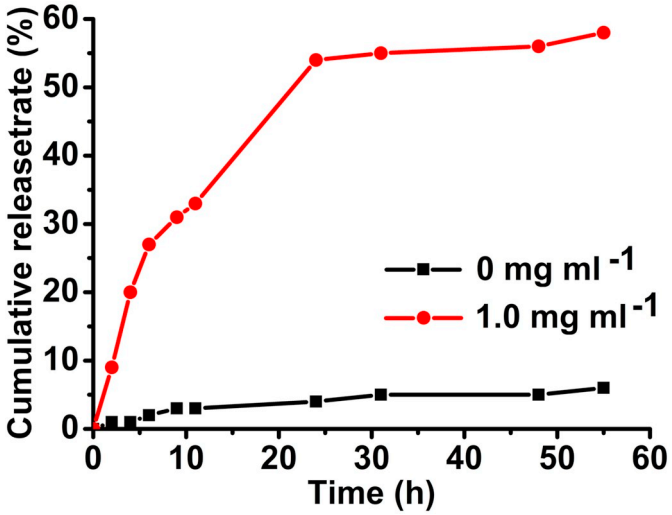

Fig. 12. In vitro release profile of RhB from micelles **β-CD@11** using $FeCl_3$ as oxidant at 0 and 1.0 mg ml^{-1}.

shown in Fig. 12, the release of RhB from micelles of **β-CD@11** is initiated by treatment with $FeCl_3$ at 1.0 mg ml^{-1}. The total release amount of RhB reaches 55% after 25 h of dialysis treatment with $FeCl_3$, and hereafter no further release is observed even after 55 h. During the dialysis treatment by $FeCl_3$, the Fc groups of Janus **11** are oxidized to cationic Fc^+ structures, and this transformation results in the weakening of the binding between β-CD and **11**. Thereby, their inclusion complexes are disintegrated and the micelle expanded due to the enhancement of the coulombic repulsion force in the cores [16]. Thus, the loaded RhB runs away from the enlarged cores of micelles. Based on the above release feature, this supramolecular micellar ensemble is anticipated to have potential applications in the fields of sustained drug delivery systems [44,81].

4. Conclusion

The design and facile synthesis of a new supramolecular Janus system with a redox response based on the inclusion complexation of Fc groups into β-CD is reported here. A typical chemo selective coupling method is successfully used for the efficient synthesis of a new bis-Fc-terminated Janus molecule containing three hydrophilic triethylene glycol branches. The new bimetallic Janus molecule is then employed as a building block to fabricate a supramolecular Janus device through the strong host-guest interaction between Fc group and β-CD at 1:1 M ratio. The successful fabrication of this supramolecular device is confirmed using one-dimensional ^1H NMR and two-dimensional nuclear Overhauser enhancement spectroscopy. The supramolecular Janus ensemble self-assembles into nearly spherical micelles on nanoscale in the aqueous system. The reversible expansion and contraction of these supramolecular micelles, as indicated by SEM and DLS, are initiated by the oxidation and reduction of Fc moieties that control the host-guest interaction of Fc with β-CD. The redox-responsive supramolecular Janus system is successfully applied to the encapsulation of model RhB cargo, and the loaded molecules slips out from the micelles upon adding the oxidant $FeCl_3$. This work provides a good example of rational design of supramolecular Janus molecules by host–guest inclusion between β-CD and Fc groups, and the present supramolecular micelles have the potential of inducing progress in the field of redox-responsive cargo delivery systems.

Abbreviations

β-CD	β-cyclodextrin
Fc	ferrocene
PDMA	poly(*N*,*N*-dimethylacrylamide)
PDEA	poly(*N*,*N*-diethylacrylamide)
PAMAM	poly(amidoamine)
Ad	adamantane
Fc^+	ferricinium
ROS	reactive oxygen species
GSH	glutathione
TEG	triethylene glycol
NOSEY	Nuclear Overhauser Enhancement Spectroscopy
SEM	scanning electron microscopy
DLS	dynamic light scattering
RhB	Rhodamine B
MWCO	molecular weight cutoff
LC	loading content
EE	encapsulation efficiency
CuAAC	copper(I)-catalyzed azide alkyne cycloaddition
Cp	cyclopentadienyl
DMSO	dimethyl sulfoxide
CMC	critical micelle concentration
PDI	polydispersity index
Δδ	shift change
NOE	Nuclear Overhauser Effect

Acknowledgements

We thank Ms. Wang Zhonghui (College of Light Industry, Textile and Food Engineering, Sichuan University) for her great help in AFM and DLS measurements and the ceshigo (www.ceshigo.com) for help in SEM. The financial support from the Science and Technology Department of Sichuan Province (No. 2018HH0038), the University of Bordeaux and the Centre National de la Recherche Scientifique (CNRS) are gratefully acknowledged.

Notes

The authors declare no competing financial interest.

Appendix A. Supplementary data

The electronic supplementary information contains the syntheses,

spectra, calculation of the number of Fc units in the dendrimer **11** and references (PDF). Supplementary data associated with this article can be found in the online version, at https://doi.org/10.1016/j.jinorgbio.2018.12.018.

References

[1] H.J. Sun, S. Zhang, V. Percec, Chem. Soc. Rev. 44 (2015) 3900–3923.
[2] K.R. Raghupathi, J. Guo, O. Munkhbat, P. Rangadurai, S. Thayumanavan, Acc. Chem. Res. 47 (2014) 2200–2211.
[3] A.-M. Caminade, R. Laurent, B. Delavaux-Nicot, J.-P. Majoral, New J. Chem. 36 (2012) 217–226.
[4] D.R. Sikwal, R.S. Kalhapure, T. Govender, Eur. J. Pharm. Sci. 97 (2017) 113–134.
[5] V. Percec, M.R. Imam, M. Peterca, P. Leowanawat, J. Am. Chem. Soc. 134 (2012) 4408–4420.
[6] J.W. Choi, B.K. Cho, Soft Matter 7 (2011) 4045–4049.
[7] J. Liu, Y. Feng, Y. He, N. Yang, Q.H. Fan, New J. Chem. 36 (2012) 380–385.
[8] T. Tuuttila, J. Lipsonen, M. Lahtinen, J. Huuskonen, K. Rissanen, Tetrahedron 64 (2008) 10590–10597.
[9] M. Filippi, D. Patrucco, J. Martinelli, M. Botta, P. Castro-Hartmann, L. Tei, E. Terreno, Nanoscale 7 (2015) 12943–12954.
[10] C. Dengiz, B. Breiten, J.P. Gisselbrecht, C. Boudon, N. Trapp, W.B. Schweizer, F. Diederich, J. Org. Chem. 80 (2015) 882–896.
[11] R.L. Tang, S.M. Zhou, Z.Y. Cheng, G. Yu, Q. Peng, H.H. Zeng, G.C. Guo, Q.Q. Li, Z. Li, Chem. Sci. 8 (2017) 340–347.
[12] M. Peterca, V. Percec, P. Leowanawat, A. Bertin, J. Am. Chem. Soc. 133 (2011) 20507–20520.
[13] Q. Xiao, S.E. Sherman, S.E. Wilner, X. Zhou, C. Dazen, T. Baumgart, E.H. Reed, D.A. Hammer, W. Shinoda, M. Klein, V. Percec, Proc. Natl. Acad. Sci. U. S. A. 114 (2017) E7045–E7053.
[14] S. Nummelin, M. Selin, S. Legrand, J. Ropponen, J. Seitsonen, A. Nykänen, J. Koivisto, J. Hirvonen, M.A. Kostiainen, L.M. Bimbo, Nanoscale 9 (2017) 7189–7198.
[15] A. Lancelot, R. Clavería-Gimeno, A. Velázquez-Campoy, O. Abian, J.L. Serrano, T. Sierra, Eur. Polym. J. 90 (2017) 136–149.
[16] L. Zhao, Q.J. Ling, X. Liu, C.D. Hang, Q.X. Zhao, F.F. Liu, H.B. Gu, Appl. Organomet. Chem. 32 (2018) e4000.
[17] C. Ornelas, J. Ruiz, E. Cloutet, S. Alves, D. Astruc, Angew. Chem. Int. Ed. 46 (2007) 872–877.
[18] G.-R. David, P.H.J.S. Albertus, Chem. Mater. 23 (2011) 310–325.
[19] X.D. Chi, G.C. Yu, L. Shao, J.Z. Chen, F.H. Huang, J. Am. Chem. Soc. 138 (2016) 3168–3174.
[20] M.M. Zhang, X.Z. Yan, F.H. Huang, Z.B. Niu, H.W. Gibson, Acc. Chem. Res. 47 (2014) 1995–2005.
[21] S.Y. Dong, B. Zheng, F. Wang, F.H. Huang, Acc. Chem. Res. 47 (2014) 1982–1994.
[22] Z. Hou, W. Dehaen, J. Lyskawa, P. Woisel, R. Hoogenboom, Chem. Commun. 53 (2017) 8423–8426.
[23] Z.F. Sun, F.C. Lv, L.J. Cao, L. Liu, Y. Zhang, Z.G. Lu, Angew. Chem. Int. Ed. 54 (2015) 7944–7948.
[24] M. Haring, D.D. Diaz, Chem. Commun. 52 (2016) 13068–13081.
[25] A. Harada, S. Takahashi, J. Chem. Soc. Chem. Commun. 10 (1984) 645–646.
[26] A. Ueno, F. Moriwali, T. Matsue, T. Osa, F. Hamada, K. Murai, Makromol. Chem. Rapid Commun. 6 (1985) 231–233.
[27] T. Matsue, D.H. Evans, T. Osa, N. Kobayashi, J. Am. Chem. Soc. 107 (1985) 3411–3417.
[28] A.E. Kaifer, Acc. Chem. Res. 32 (1999) 62–71.
[29] A. Harada, Acc. Chem. Res. 34 (2001) 456–464.
[30] M. Nakahata, Y. Takashima, H. Yamaguchi, A. Harada, Nat. Commun. 511 (2011).
[31] B.V.K.J. Schmidt, D. Kugele, J. von Irmer, J. Steinkoenig, H. Mutlu, C. Rüttiger, C.J. Hawker, M. Gallei, C. Barner-Kowollik, Macromolecules 50 (2017) 2375–2386.
[32] F. Chen, L.D. Kong, L. Wang, Y. Fan, M.W. Shen, X.Y. Shi, J. Mater. Chem. B 5 (2017) 8459–8466.
[33] G.Y. Li, Z.R. Dong, Y.T. Zhu, W.J. Tong, C.Y. Gao, J. Colloid Interface Sci. 475 (2016) 196–202.
[34] E. Wajs, T.T. Nielsen, K.L. Larsen, A. Fragoso, Nano Res. 9 (2016) 2070–2078.
[35] Q. Yan, J.Y. Yuan, Z.N. Cai, Y. Xin, Y. Kang, Y.W. Yin, J. Am. Chem. Soc. 132 (2010) 9268–9270.
[36] Y. Kang, Y. Ma, S. Zhang, L.S. Ding, B.J. Li, ACS Macro Lett. 4 (2015) 543–547.
[37] C. Zuo, X.Y. Dai, S.J. Zhao, X.N. Liu, S.L. Ding, L.W. Ma, M.Z. Liu, H. Wei, ACS Macro Lett. 5 (2016) 873–878.
[38] Y. Wang, H.B. Wang, Y.J. Chen, X.S. Liu, Q. Jin, J. Ji, Colloids Surf. B Biointerfaces 121 (2014) 189–195.
[39] Y. Zhang, J.K. Duan, L.G. Cai, D. Ma, W. Xue, ACS Appl. Mater. Interfaces 8 (2016) 29343–29355.
[40] X.J. Loh, Mater. Horiz. 1 (2014) 185–195.
[41] Q.D. Hu, G.P. Tang, P.K. Chu, Acc. Chem. Res. 47 (2014) 2017–2025.
[42] B.V.K.J. Schmidt, M. Hetzer, H. Ritter, C. Barner-Kowollik, Prog. Polym. Sci. 39 (2014) 235–249.
[43] L. Peng, A.C. Feng, M. Huo, J.Y. Yuan, Chem. Commun. 50 (2014) 13005–13014.
[44] H.B. Gu, S.D. Mu, G.R. Qiu, X. Liu, L. Zhang, Y.F. Yuan, D. Astruc, Coord. Chem. Rev. 364 (2018) 51–85.
[45] L. Peng, S.Y. Liu, A.C. Feng, J.Y. Yuan, Mol. Pharm. 14 (2017) 2475–2486.
[46] F. Szillat, B.V.K.J. Schmidt, A. Hubert, C. Barner-Kowollik, H. Ritter, Macromol. Rapid Commun. 35 (2014) 1293–1300.
[47] F. Li, T. Ito, J. Am. Chem. Soc. 135 (2013) 16260–16263.
[48] T. Gao, L.D. Li, B. Wang, J. Zhi, Y. Xiang, G.X. Li, Anal. Chem. 88 (2016) 9996–10001.
[49] M. Gade, A. Paul, C. Alex, D. Choudhury, H.V. Thulasiram, R. Kikkeri, Chem. Commun. 51 (2015) 6346–6349.
[50] L. Peng, A.C. Feng, S.Y. Liu, M. Huo, T. Fang, K. Wang, Y. Wei, X.S. Wang, J.Y. Yuan, ACS Appl. Mater. Interfaces 8 (2016) 29203–29207.
[51] G. Xu, D. Pranantyo, L.Q. Xu, K.G. Neoh, E.-T. Kang, S.L.-M. Teo, Ind. Eng. Chem. Res. 55 (2016) 10906–10915.
[52] F. Wang, H.T. Pu, X. Che, Chem. Commun. 52 (2016) 3516–3519.
[53] K. Miyamae, M. Nakahata, Y. Takashima, A. Harada, Angew. Chem. Int. Ed. 54 (2015) 8984–8987.
[54] Y. Kang, X. Ju, L.S. Ding, S. Zhang, B.J. Li, ACS Appl. Mater. Interfaces 9 (2017) 4475–4484.
[55] S. Nlate, J. Ruiz, J.-C. Blais, D. Astruc, Chem. Commun. (2000) 417–418.
[56] G.R. Newkome, C.D. Shreiner, Chem. Rev. 110 (2010) 6338–6442.
[57] D. Astruc, E. Boisselier, C. Ornelas, Chem. Rev. 110 (2010) 1857–1959.
[58] C.M. Casado, B. Alonso, J. Losada, M.P. Garcia-Armada, S. Campana, P. Ceroni, F. Puntoriero (Eds.), Designing Dendrimers, Wiley, Hoboken, NJ, 2012, pp. 219–262.
[59] D. Astruc, Nat. Chem. 4 (2012) 255–267.
[60] D. Astruc, Eur. J. Inorg. Chem. (2017) 6–29.
[61] Y.R. Leroux, H. Fei, J.M. Noël, P. Hapiot, J. Am. Chem. Soc. 132 (2010) 14039–14041.
[62] X. Liu, S.D. Mu, G.R. Qiu, Y.R. Long, Q.J. Ling, J.J. He, H.B. Gu, Polymer 146 (2018) 275–290.
[63] J. Ruiz, D. Astruc, C.R. Acad. Sci., Ser. IIc 1 (1998) 21–27.
[64] I. Noviandri, K.N. Brown, D.S. Fleming, P.T. Gulyas, P.A. Lay, A.F. Masters, L. Phillips, J. Phys. Chem. B 103 (1999) 6713–6722.
[65] J. Ruiz, M.-C. Daniel, D. Astruc, Can. J. Chem. 84 (2006) 288–299.
[66] J.B. Flanagan, S. Margel, A.J. Bard, F.C. Anson, J. Am. Chem. Soc. 100 (1978) 4248–4253.
[67] X. Liu, Q.J. Ling, L. Zhao, G.R. Qiu, Y.H. Wang, L.X. Song, Y. Zhang, J. Ruiz, D. Astruc, H.B. Gu, Macromol. Rapid Commun. 38 (2017) 1700448.
[68] G.R. Qiu, L. Zhao, X. Liu, Q.X. Zhao, F.F. Liu, Y. Liu, Y.W. Liu, H.B. Gu, React. Funct. Polym. 128 (2018) 1–8.
[69] Y. Liu, S.D. Mu, X. Liu, Q.J. Ling, C.D. Hang, J. Ruiz, D. Astruc, H.B. Gu, Tetrahedron 74 (2018) 4777–4789.
[70] V.V. Rostovtsev, L.G. Green, V.V. Fokin, K.B. Sharpless, Angew. Chem. Int. Ed. 41 (2002) 2596.
[71] L. Zhao, X. Liu, L. Zhang, G.R. Qiu, D. Astruc, H.B. Gu, Coord. Chem. Rev. 337 (2017) 34–79.
[72] N.G. Connelly, W.E. Geiger, Chem. Rev. 96 (1996) 877–910.
[73] A.K. Diallo, J.-C. Daran, F. Varret, J. Ruiz, D. Astruc, Angew. Chem. Int. Ed. 48 (2009) 3141–3145.
[74] A.K. Diallo, C. Absalon, J. Ruiz, D. Astruc, J. Am. Chem. Soc. 133 (2011) 629–641.
[75] H.B. Gu, R. Ciganda, P. Castel, S. Moya, R. Hernandez, J. Ruiz, D. Astruc, Angew. Chem. Int. Ed. 57 (2018) 2204–2208.
[76] L. Zhang, G.R. Qiu, F.F. Liu, X. Liu, S.D. Mu, Y.R. Long, Q.X. Zhao, Y. Liu, H.B. Gu, React. Funct. Polym. 132 (2018) 60–73.
[77] X. Liu, G.R. Qiu, L. Zhang, F.F. Liu, S.D. Mu, Y.R. Long, Q.X. Zhao, Y. Liu, H.B. Gu, Macromol. Chem. Phys. 219 (2018) 1800273.
[78] H.J. Schneider, F. Hacket, V. Rüdiger, H. Ikeda, Chem. Rev. 98 (1998) 1755–1785.
[79] B.V.K.J. Schmidt, T. Rudolph, M. Hetzer, H. Ritter, F.H. Schacher, C. Barner-Kowollik, Polym. Chem. 3 (2012) 3139–3145.
[80] L.C. Liu, L.L. Rui, Y. Gao, W.A. Zhang, Polym. Chem. 6 (2015) 1817–1829.
[81] G. Saravanakumar, J. Kim, W.J. Kim, Adv. Sci. 4 (2017) 1600124.